ChemComm

ROYAL SOCIETY OF CHEMISTRY

COMMUNICATION

View Article Online
View Journal | View Issue

Cite this: *Chem. Commun.*, 2024, **60**, 10362

Received 24th May 2024,
Accepted 22nd August 2024

DOI: 10.1039/d4cc02536a

rsc.li/chemcomm

Construction of binary metal–organic cage-based materials *via* a "covalently linked plus cage encapsulated" strategy†

Pei Lai, Jia-Xuan Wu, Liang-Hua Wu, Lai-Yi Li, Song-Liang Cai and Sheng-Run Zheng *

A strategy for constructing binary metal–organic cage (MOC)-based materials was developed. The cationic MOCs were covalently linked by organic linkers to a cationic extended network, whereas the anionic MOCs acted as counterions and were encapsulated in the network. Compared with the corresponding unary materials, the binary MOC-based materials exhibited improved porosity and adsorption performance.

Metal–organic cages (MOCs), also called metal–organic polyhedrons (MOPs), or porous coordination cages (PCCs), are discrete coordination molecules with three-dimensional cavities that have diverse applications in guest binding,[1,2] catalysis,[3,4] biological imaging,[5] drug delivery,[6] enantiomer separation,[7] and so on. The discrete nature, solubility and stability of MOCs allow these coordination molecules to be considered building blocks for further construction of functional materials such as metal–organic frameworks (MOFs), gels, and membranes.[8–12] Such a strategy means that nanosize coordination cavities could be introduced *via* presynthesized MOCs; thus, it is more predictable and easier to establish structural–property relationships. To increase the complexity of the supramolecular framework based on the type of coordination cavity, this strategy also provides a convenient route if two or more MOCs are used as starting reactants.[13] However, there are only a few reports on this topic, and this topic remains largely unexplored.[13–16]

For incorporating two or more MOCs into a unique material, the reported strategies are shown in Scheme 1. In strategy **I**, a cationic MOC and an anionic MOC can result in MOC-based porous salts containing these two MOCs *via* metathesis reactions.[14–16] In strategy **II**, two different MOCs were covalently or coordinately linked to a network with two MOCs.[13] In addition, the crystallization of a MOC mixture with the same structural type but ligands with different substituent groups led to an MOC supramolecular framework with various MOCs; such a strategy is called a multivariate strategy (strategy **III**).[17] In strategies **I** and **III**, interactions among the MOCs are weak, and the MOCs may break away from the framework. In strategy **II**, interactions among MOCs were stronger, but small counterions may occupy the cavities in the network because the charges of the two MOCs were the same, thereby reducing their adsorption performance. Herein, by combining the advantages of strategies **I** and **II**, a new strategy for synthesizing binary MOC-based materials has been developed. As shown in Scheme 1, the cationic MOC was covalently linked to form a cationic extended network in which the cationic MOCs were tightly incorporated. An anionic MOC with the opposite charge was introduced to replace small inorganic anions. Due to the strong electrostatic interaction between

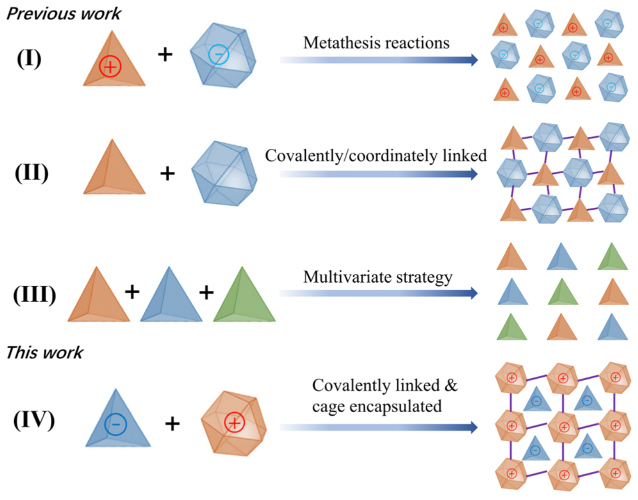

Scheme 1 Strategies for constructing binary metal–organic cage (MOC)-based materials.

GDMPA Key Laboratory for Process Control and Quality Evaluation of Chiral Pharmaceuticals, and Guangzhou Key Laboratory of Analytical Chemistry for Biomedicine, School of Chemistry, South China Normal University, Guangzhou 510006, China. E-mail: zhengsr-scnu.edu.cn, songliangcai@m.scnu.edu.cn; Fax: +86-20-39310210

† Electronic supplementary information (ESI) available: See DOI: **https://doi.org/10.1039/d4cc02536a**

the highly charged cationic and anionic MOCs, the anionic MOCs were expected to be steadily incorporated into the network, thereby giving rise to binary MOC-based materials.

As shown in Scheme 2, to achieve this strategy, a cationic $Pd_{12}L_{24}$ (L = 3,5-di-pyridin-4-yl-benzaldehyde, Pd-MOC) cage with a peripheral aldehyde group was employed to construct the MOC-based extended network. This Pd-MOC has been used as an effective building block for preparing MOC-based gels or amorphous solids *via* the condensation of aldimine with various amines.[18–20] In addition, it has been proven that this cage is stable under solid-state reaction conditions as indicated by 1H NMR before and after grinding for 1 h (Fig. S1, ESI†).[20] To link these Pd-MOCs, a triamine with a large spacer, 5″-(4′-amino-[1,1′-biphenyl]-4-yl)-[1,1′:4′,1″:3″,1‴:4‴,1⁗-quinque-phenyl]-4,4⁗-diamine (TA), was employed. Owing to the poor solubility of Pd-MOC in common solvents used for aldimine condensation and the successful generation of two similar products through solid-phase synthesis,[19,20] herein, the reaction of Pd-MOC with TA was also performed by grinding. The resulting cationic extended MOC-based amorphous solid (Pd-MOC-TA), as revealed by various characterization methods. In the IR spectra (Fig. S2, ESI†), the peak at 1701 cm^{-1} assigned to the C=O of the aldehyde group and the peak assigned to the amino group at 3364 cm^{-1} were lower than those in the linker and the Pd-MOC spectra, suggesting that a reaction between the aldehyde group and amino group occurred. In addition, the peak at 1385 cm^{-1} for NO_3^- remained. From the Raman spectrum (Fig. S3, ESI†), the relative intensity of the peak at 1604 cm^{-1} assigned to the C=N bond increased,[20] also indicating the presence of newly generated C=N bonds in Pd-MOC-TA. According to the C 1s XPS spectra (Fig. S4, ESI†), the C=O fraction decreased, and the C=N fraction increased, which further supported the successful linkage of Pd-MOC by the linker under such conditions. The N 1s spectrum showed an increase in the C=N fraction and the retention of the NO_3^- anion (Fig. S5, ESI†). The resulting solid is amorphous, as shown in Fig. S6 (ESI†). In contrast to Pd-MOC, it is almost insoluble in DMSO. SEM showed that it was composed of irregular nanosized particles that aggregated together (Fig. S7, ESI†). EDS showed a homogeneous distribution of Pd (Fig. S8, ESI†). Small-angle X-ray scattering (SAXS, Fig. S9, ESI†) indicated that the peak for the cage in Pd-MOC remained in Pd-MOC-TA, which is similar to materials based on a similar cage.[18] This result further confirmed that the cage structure was retained during the reaction. The zeta potential of Pd-MOC-TA is 45.1 mV, which is slightly greater than that of Pd-MOC (Fig. S10, ESI†). This high zeta potential may be due to the high positive charge of Pd-MOC and the release of some NO_3^- on its surface. The nitrogen adsorption–desorption isotherms at 77 K indicate that the BET surface area of Pd-MOC-TA is only 16.2 cm^3 g^{-1} (Fig. S11a, ESI†). This may be because the network of Pd-MOC-TA is cationic, in which the cavities may be occupied by nonporous NO_3^- anions, and because of the amorphous nature of Pd-MOC-TA.[21] The pore size distribution (Fig. S11b, ESI†) indicates that there may be some pores in the mesoporous range among the MOCs.

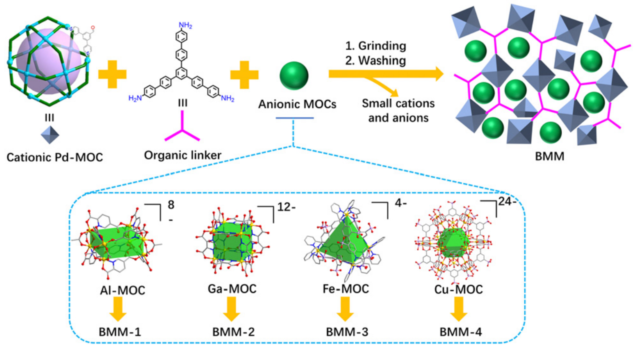

Scheme 2 Construction of the binary metal–organic cage (MOC)-based materials BMM-1 to BMM-4.

Four anionic MOCs with different shapes and charges, $[Al_8(pdc)_8(OAc)_8O_4]^{8-}$ (H_2pdc = 2,5-pyridinedicarboxylic acid, Al-MOC),[22] $[Ga_8(ImDC)_{12}]^{12-}$ (H_3ImDC = 4,5-imidazoledicarboxylic acid, Ga-MOC),[23] $[Fe_4(L)_6]^{4-}$ (H_2L = 4,4′-bis(((*E*)-pyridin-2-ylmethylene)amino)-[1,1′-biphenyl]-2,2′-disulfonic acid, Fe-MOC),[24] and $[Cu_{24}(SO_3\text{-bdc})_{24}]^{24-}$ (HSO_3-bdc = 5-sulfo-1,3-benzenedicarboxylic, Cu-MOC),[25] were used for incorporation into the Pd-MOC-TA network (Scheme 2). These MOCs have been synthesized according to the literature,[22–25] and obviously do not contain any functional groups for covalent linking with TA. The stability of these cages under grid conditions was studied, as shown in Fig. S12–S15 (ESI†). After 1 h of grinding, the molecular cage structures were retained, as revealed by ^{1}H NMR or UV-vis spectroscopy. We first attempted to incorporate them into the Pd-MOC-TA network by anion exchange with NO_3^- in solution, but these reactions were not successful, as seen from the IR spectra, as the peak for NO_3^- was still significantly observed (Fig. S16, ESI†), possibly due to the lack of significant channels available for dispersing the large anionic MOCs into the inner network of Pd-MOC-TA but located only on its surface. Thus, we attempted to incorporate them *in situ* during the synthesis process. The one-pot reactions with Pd-MOC, TA, and anionic MOCs (Al-MOC, Ga-MOC, Fe-MOC, and Cu-MOC) resulted in four binary MOC-based solids, namely, BMM-1, BMM-2, BMM-3, and BMM-4, respectively (Scheme 2). The characterization and analysis of BMM-1, BMM-2, BMM-3, and BMM-4 are similar; therefore, we mainly describe them with BMM-1 as the representative. As shown in Fig. 1a and Fig. S17–S19 (ESI†), the IR spectra indicate that they possess peaks attributed to both Pd-MOC-TA and the anionic MOCs. For BMM-1, the peaks assigned to the stretching vibrations of C=O, C=N and C=C (1600 to 1700 cm^{-1}) and the bending vibrations of C–O and $-CH_3$ (1411 and 1351 cm^{-1}) from Al-MOC show some shifts in BMM-1 (Fig. 1a), indicating interactions between Al-MOC and the cationic Pd-MOC-based framework. In addition, the strong peak at 1382 cm^{-1} assigned to NO_3^- in Pd-MOC-TA decreased/disappeared in BMM-1, implying that NO_3^- was replaced by anionic MOCs; thus, the incorporation of anionic MOCs was successful. The absence of NO_3^- was further confirmed by the N 1s XPS spectra (Fig. 1b and Fig. S20–S22, ESI†), in which no peaks can be attributed to NO_3^- (when compared with the N 1s spectra in Fig. 1d, the conclusion is more certain). The XPS full spectra of the BMMs also indicate the presence of two types of metal ions from the two MOCs (Fig. 1c and Fig. S23–S25, ESI†). For BMM-3 and BMM-4, S was also observed, further confirming the

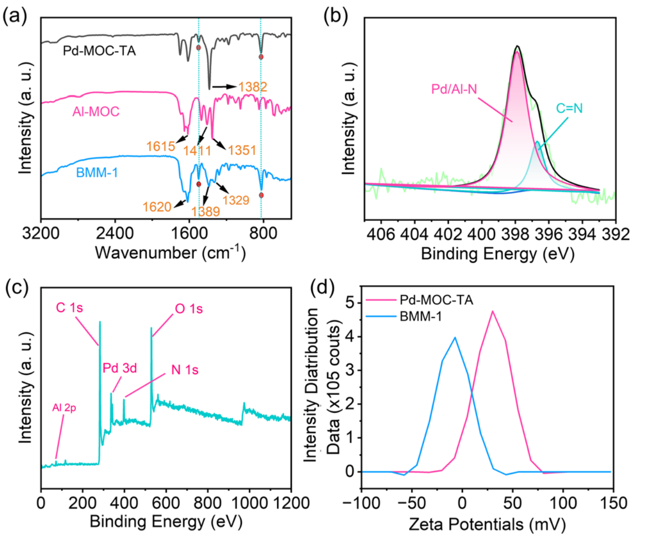

Fig. 1 (a) IR spectra of Pd-MOC-TA, Al-MOC, and BMM-1. (b) The N 1s XPS spectra of BMM-1. (c) XPS full spectrum of BMM-1. (d) ζ-Potential of Pd-MOC-TA and BMM-1.

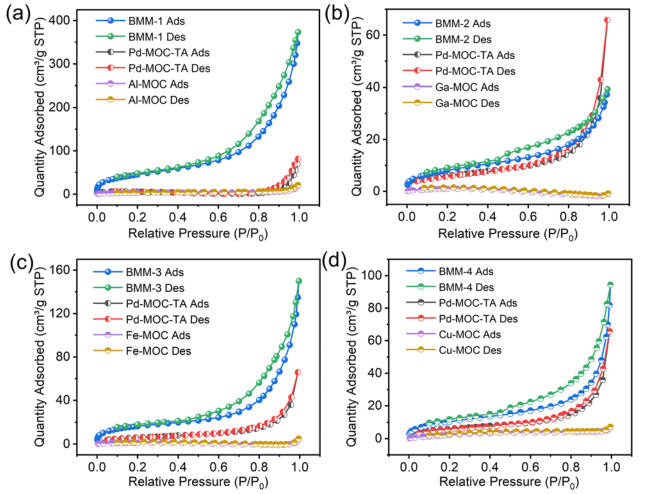

Fig. 2 Comparisons of the N_2 adsorption isotherms at 77 K for (a) BMM-1, (b) BMM-2, (c) BMM-3, and (d) BMM-4 with those of Pd-MOC-TA and unary MOC-based materials based on their corresponding anionic MOCs.

incorporation of anionic MOCs. The ratios of the two metal ions were determined by ICP. The results are shown in Table S1 (ESI†). These ratios were approximately equal to the ratios calculated according to the charge balance requirements of cationic Pd-MOC and anionic MOCs in BMM-3 and BMM-4. However, in BMM-1 and BMM-2, the anionic MOCs are slightly excessive, possibly because Al-MOC and Ga-MOC are smaller and have a large number of carboxyl groups on the periphery, which allows them to not only replace NO_3^- but also embed in the network through weak interactions. SEM showed that the morphology of the BMMs was similar to that of Pd-MOC-TA (Fig. S26–S29, ESI†). EDS showed that the Pd and metal ions from anionic MOCs were distributed homogeneously in these binary MOC-based solids (Fig. S30–S33, ESI†). After the NO_3^- was replaced by anionic MOCs, the zeta potential of the resulting BMMs was nearly neutral, which is significantly lower than that of Pd-MOC-TA (Fig. 1d and Fig. S24–S36, ESI†), possibly because the release of large anionic MOCs with large sizes and large negative changes is more difficult than that of NO_3^-. It has been shown that cationic Pd-MOC-based materials with NO_3^- counterions exhibit good performance in the removal of $Cr_2O_7^{2-}$ *via* anion exchange and framework absorption.[19] Thus, $Cr_2O_7^{2-}$ adsorption in water by Pd-MOC-TA and the four BMMs was carried out and compared (Fig. S37, ESI†). The removal rate of the BMMs was obviously lower than that of Pd-MOC-TA, further indicating the lack of exchangeable NO_3^- and the tight incorporation of anionic MOCs in the network of BMMs.

Because anionic MOCs have a greater charge than NO_3^- and contain cavities, we speculate that the resulting BMM may show improved porosity and adsorption performance compared with the anionic bulk MOC and Pd-MOC-TA. The four amorphous anionic MOC solids showed no response to N_2 due to the random packing of these MOCs,[26,27] the presence of counterions, and the small size of the anionic MOC (except for Cu-MOC). However, for the BMM solid, the BET surface area increased to some extent. The BET surface areas of BMM-1, BMM-2, BMM-3, and BMM-4 are 167.3, 33.8, 59.3, and 39.8 cm^3 g^{-1}, respectively, as shown in Fig. 2. In addition, larger H3 hysteresis loops were observed for the BMMs, indicating their mesoporosity. The increase in the porosity of the BMMs compared with that of their corresponding amorphous anionic MOCs and Pd-MOC-TA is likely attributed to the decrease in the number of small inorganic anions/cationic number compared with that of the original unary MOC-based materials and is similar to that of MOC-based porous salts.[14–16] These results also support the incorporation of anionic MOCs in the framework because the BET surface area cannot be increased when the anionic MOC is absorbed only on the surface.[28] The N_2 adsorption–desorption isotherm of the product obtained from the immersion of Pd-MOC-TA in the Al-MOC solution and the mixture of Pd-MOC-TA and Al-MOC was measured and compared, and the results revealed that its BET surface area was still very low in these two case (Fig. S38, ESI†).

In addition, the ability of these materials to adsorb methanol molecules in saturated methanol vapour at room temperature was also preliminarily studied using a quartz crystal microbalance (QCM).[29,30] The mass of the sample and its adsorbed methanol were measured by frequency variation on a QCM. The setup is shown in Fig. S39 (ESI†). The results are shown in Fig. 3. The adsorption capacity of unary Pd-MOC-TA was 0.315 g g^{-1}. The maximum saturated adsorption capacities of BMM-1, BMM-2, BMM-3, and BMM-4 were 0.405, 0.512, 0.832, and 1.12 g g^{-1}, respectively, which are significantly greater than that of Pd-MOC-TA. This indicates that the replacement of NO_3^- by highly negatively charged porous MOCs indeed has a positive influence on the adsorption performance. The introduction of anionic MOCs leads to an increase in adsorption capacity mainly because, on the one hand, each anionic MOC can exchange multiple nitrate ions due to its high negative charge, thereby releasing some internal cavities; on the other hand, anionic MOCs themselves also have some cavities. In addition, the interaction sites will also be altered by the introduction of anionic MOCs. For BMM-1 and BMM-2, the cavity and window size of the anionic MOCs are too small to

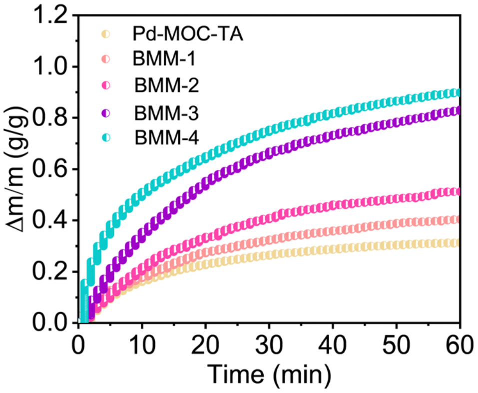

Fig. 3 The methanol adsorption capacities at 298 K for BMM-1, BMM-2, BMM-3, BMM-4, and Pd-MOC-TA *via* QCM.

absorb methanol molecules; thus, the improvement in methanol adsorption capacity is relatively small. In BMM-4, the cavity of Cu-MOC is relatively large; therefore, the adsorption capacity is significantly increased. However, due to the amorphous nature of these materials, their structural details are difficult to determine; thus, it is currently difficult for us to establish a clear relationship between methanol adsorption performance and structure, which will be further studied in the future.

In conclusion, four BMMs containing two types of MOCs with opposite charges were constructed by a new ''covalently linked plus cage-encapsulated'' strategy. The porosity and methanol adsorption capacities of these materials were improved in most cases compared with those of their corresponding unary MOC-based materials. This work demonstrates a new attempt to construct functional materials with two presynthesized MOCs as building blocks, which could enrich the types of MOC-based materials. We are attempting to incorporate more types of MOC into a unique network and explore their structure–property relationships.

This work was financially supported by the National Natural Science Foundation of China (grant no. 22073032 and 92356303) and the Guangdong Basic and Applied Basic Research Foundation (Grant No. 2022A1515011243 and 2024A1515011117).

Data availability

The data supporting this article have been included as part of the ESI.†

Conflicts of interest

There are no conflicts to declare.

Notes and references

1 F. J. Rizzuto, L. K. S. von Krbek and J. R. Nitschke, *Nat. Rev. Chem.*, 2019, **3**, 204–222.
2 Y.-H. Huang, Y.-L. Lu, J. Ruan, S.-P. Zheng, X.-D. Zhang, C.-H. Liu, Y.-H. Qin, Z.-M. Cao, Z. Jiao, H.-S. Xu and C.-Y. Su, *J. Am. Chem. Soc.*, 2023, **145**, 23361–23371.
3 Y. Fang, J. A. Powell, E. Li, Q. Wang, Z. Perry, A. Kirchon, X. Yang, Z. Xiao, C. Zhu, L. Zhang, F. Huang and H.-C. Zhou, *Chem. Soc. Rev.*, 2019, **48**, 4707–4730.
4 Y.-L. Lu, J.-Q. Song, Y.-H. Qin, J. Guo, Y.-H. Huang, X.-D. Zhang, M. Pan and C.-Y. Su, *J. Am. Chem. Soc.*, 2022, **144**, 8778–8788.
5 W.-T. Dou, C.-Y. Yang, L.-R. Hu, B. Song, T. Jin, P.-P. Jia, X. Ji, F. Zheng, H.-B. Yang and L. Xu, *ACS Mater. Lett.*, 2023, **5**, 1061–1082.
6 Y.-P. Wang, Y. Zhang, X.-H. Duan, J.-J. Mao, M. Pan, J. Shen and C.-Y. Su, *Coord. Chem. Rev.*, 2024, **501**, 215570.
7 C. Liu, J. Li, M. Lu, X. Jia, A. Yu and S. Zhang, *Sep. Purif. Technol.*, 2024, **332**, 125765.
8 E. Sánchez-González, M. Y. Tsang, J. Troyano, G. A. Craig and S. Furukawa, *Chem. Soc. Rev.*, 2022, **51**, 4876–4889.
9 H. Wang, Y. Jin, N. Sun, W. Zhang and J. Jiang, *Chem. Soc. Rev.*, 2021, **50**, 8874–8886.
10 T.-T. Li, S.-N. Liu, L.-H. Wu, S.-L. Cai and S.-R. Zheng, *ChemPlusChem*, 2022, **87**, e202200172.
11 E. S. M. El-Sayed and D. Yuan, *Chem. Lett.*, 2020, **49**, 28–53.
12 A. Khobotov-Bakishev, L. Hernández-López, C. von Baeckmann, J. Albalad, A. Carné-Sánchez and D. Maspoch, *Adv. Sci.*, 2022, **9**, 2104753.
13 A. W. Markwell-Heys, M. Roemelt, A. D. Slattery, O. M. Linder-Patton and W. M. Bloch, *Chem. Sci.*, 2022, **13**, 68–73.
14 J. Gosselin, A. M. Antonio, K. J. Korman, M. M. Deegan, G. P. A. Yap and E. D. Bloch, *J. Am. Chem. Soc.*, 2021, **143**, 14956–14961.
15 S. Ogihara, T. Komatsu, Y. Itoh, Y. Miyake, T. Suzuki, K. Yanagi, Y. Kimura, T. Ueno, K. Hanaoka, H. Kojima, T. Okabe, T. Nagano and Y. Urano, *J. Am. Chem. Soc.*, 2020, **142**, 21–26.
16 K. J. Korman, M. R. Dworzak, G. P. A. Yap and E. D. Bloch, *Small*, 2023, **19**, 2207507.
17 D. Nam, J. Kim, E. Hwang, J. Nam, H. Jeong, T.-H. Kwon and W. Choe, *Matter*, 2021, **4**, 2460–2473.
18 J. Uchida, M. Yoshio, S. Sato, H. Yokoyama, M. Fujita and T. Kato, *Angew. Chem., Int. Ed.*, 2017, **56**, 14085–14089.
19 S.-Q. Deng, D.-M. Li, X.-J. Mo, Y.-L. Miao, S.-L. Cai, J. Fan, W.-G. Zhang and S.-R. Zheng, *ChemPlusChem*, 2021, **86**, 709–715.
20 S.-N. Liu, H.-N. Wang, M.-L. Feng, K.-L. Yang, S. Cai, J. Fan, W.-G. Zhang and S.-R. Zheng, *ACS Appl. Nano Mater.*, 2023, **6**, 656–663.
21 X. Jin, G.-Q. Wang, D. Ma, S.-Q. Deng, S.-L. Cai, J. Fan, W.-G. Zhang and S.-R. Zheng, *ACS Appl. Nano Mater.*, 2019, **2**, 5824–5832.
22 S. Ilic, A. M. May, P. M. Usov, H. D. Cornell, B. Gibbons, P. Celis-Salazar, D. R. Cairnie, J. Alatis, C. Slebodnick and A. J. Morris, *Inorg. Chem.*, 2022, **61**, 6604–6611.
23 P. Sutar, V. M. Suresh, K. Jayaramulu, A. Hazra and T. K. Maji, *Nat. Commun.*, 2018, **9**, 3587.
24 P. Mal, D. Schultz, K. Beyeh, K. Rissanen and J. R. Nitschke, *Angew. Chem., Int. Ed.*, 2008, **47**, 8297–8301.
25 J.-R. Li and H.-C. Zhou, *Nat. Chem.*, 2010, **2**, 893–898.
26 W. Lu, D. Yuan, A. Yakovenko and H.-C. Zhou, *Chem. Commun.*, 2011, **47**, 4968–4970.
27 M. Jaya Prakash, M. Oh, X. Liu, K. N. Han, G. H. Seong and M. S. Lah, *Chem. Commun.*, 2010, **46**, 2049–2051.
28 L. B. Sun, J.-R. Li, W. Lu, Z.-Y. Gu, Z. Luo and H.-C. Zhou, *J. Am. Chem. Soc.*, 2012, **134**, 15923–15928.
29 L. Wang, *Sens. Actuators, A*, 2020, **307**, 111984.
30 X. Peng, X. Wu, M. Zhang and H. Yuan, *ACS Sens.*, 2023, **8**, 2471–2492.